Adsorption
https://doi.org/10.1007/s10450-019-00162-x

Adsorption and diffusion of CO_2 in CPO-27–Ni beads

S. Krishnamurthy[1,2] · R. Blom[3] · M. C. Ferrari[1] · S. Brandani[1]

Received: 23 May 2019 / Revised: 14 August 2019 / Accepted: 19 August 2019

Abstract
The present work involves the scale-up and characterization of CPO-27–Ni metal organic framework using a range of experimental techniques aimed at determining equilibrium and kinetic parameters to assess its potential for post-combustion carbon capture. CPO-27–Ni was prepared from its precursors by molecular gastronomy methods in kilogram scale. Adsorption of isotherms of pure CO_2 and N_2 were obtained for different temperatures on these beads, using a volumetric apparatus and the isotherms were fitted to a dual-site Langmuir model. A series of experiments were then carried out in the volumetric apparatus by dosing a known volume of CO_2 and the pressure was monitored with time. The diffusional time constants were then extracted by fitting the series of curves to an isothermal diffusion model. From the time constants, the values of the diffusivities were obtained and compared with the values obtained from first principles correlations, which employed the pore size, and the porosity values from independent mercury porosimetry experiments. The results from the analysis showed that the transport of CO_2 in the beads was well described by a combination of Knudsen and viscous diffusion mechanisms. Experiments were also carried out using a zero-length column (ZLC) apparatus by preparing a 10% CO_2–He and 10% CO_2–N_2 mixture. The analysis of the ZLC curves showed that the two different carrier gases had an effect of the long-time slope, indicating the presence of a macropore-controlled diffusion mechanism.

Keywords Beaded CPO-27 · CO_2 adsorption · CO_2 diffusion · Volumetric · Zero length column

1 Introduction

Metal organic frameworks (MOFs) are a new class of materials, which have a high surface area and a large pore volume (Furukawa et al. 2013). Due to these characteristics, these materials have found extensive applications such as gas storage (Gygi et al. 2016; Mason et al. 2014; Tagliabue et al. 2011), heterogeneous catalysis (Pettinari et al. 2017; Ranocchiari and van Bokhoven 2011), adsorption desalination (Youssef et al. 2017), respiratory filters (Hindocha and Poulston 2017), drug delivery systems (Al Haydar et al. 2017; Pettinari et al. 2017), sensors (Lustig et al. 2017; Pettinari et al. 2017), MOF–polymer composites (Zhang et al. 2016), etc.

One of the widely studied MOFs is the CPO-27–Ni, also known as the Ni-dobdc MOF, in which a divalent Ni cation is co-ordinated to 2, 5-dioxidoterephthalate linker (Dietzel et al. 2010). This material possesses open metal sites, which can interact with different gas molecules and a potential application for this material is to capture and concentrate CO_2 from post-combustion flue gas streams (Dietzel et al. 2009; Pato-Doldán et al. 2017).

Several published studies exist in literature, which have studied the adsorption of CO_2 in CPO-27–Ni. It has been found that this material possess a very high CO_2 capacity comparable and in some cases superior to that of Zeolite 13X, the current benchmark material for CO_2 capture applications (Dietzel et al. 2009; Pato-Doldán et al. 2017). The other issue with Zeolite 13X is that the CO_2 adsorption capacity is significantly reduced in the presence of water vapour and this can affect the performance of an adsorption process designed to capture CO_2 from wet flue gas streams (Krishnamurthy et al. 2014a; Li et al. 2008). CPO-27–Ni is a stable MOF which can retain its capacity under long term storage (Liu et al. 2011) and the material can retain from 60 up to 85% of the original CO_2

✉ S. Brandani
s.brandani@ed.ac.uk

[1] School of Engineering, The University of Edinburgh, Kings Buildings, Mayfield Road, Edinburgh EH9 3FB, UK

[2] Present Address: SINTEF Industry, Forskningsveien 1, Oslo, Norway

[3] SINTEF Industry, Forskningsveien 1, Oslo, Norway

Published online: 29 August 2019

capacity when exposed to water vapour (Hu et al. 2018; Kizzie et al. 2011; Liu et al. 2010; Mangano et al. 2016).

In a post-combustion capture process, from a coal-fired power plant, the flue gas contains around 12–15% CO_2 along with a large amount of nitrogen (Krishnamurthy et al. 2014b). The challenge is to concentrate the CO_2 to over 90%, with a high recovery, minimum energy consumption and maximum productivity (Khurana and Farooq 2016; Krishnamurthy et al. 2014b). In order to achieve the desired targets, a suitable adsorbent with high CO_2 capacity, high CO_2 and N_2 selectivity and fast mass transfer is needed. Most of the literature on CO_2 adsorption in CPO-27–Ni and other MOFs focus on CO_2 adsorption equilibrium with minimal information on mass transfer. To the best of our knowledge, only Liu et al. (2010) and Hu et al. (2015b), have studied the mass transfer mechanism on CPO-27–Ni beads. In case of Liu et al. (2010), uptake experiments were carried out with different bead sizes, by frequency response technique, while Hu et al. (2015b), studied CO_2 adsorption mechanism using a zero-length column (ZLC) method. Both these studies concluded that the mass transfer mechanism was controlled by the diffusion in macropores. As mentioned before, selectivity is also an important criterion to select an adsorbent. It has been shown by Rajagopalan et al. (2016), that the nitrogen adsorption plays a pivotal role in determining the performance of a carbon capture process. In the case of CPO-27–Ni, limited information on nitrogen adsorption exists in literature and the aim of this study is to address these gaps in order to evaluate the suitability of this material for adsorption-based carbon capture.

For the first time, SINTEF had synthesized the Ni MOF beads in kilogram quantities. Single component CO_2 and N_2 isotherms were measured on these beads using a volumetric apparatus. In the next step, the mass transfer mechanism was studied using volumetric and ZLC experiments. Independent mercury intrusion experiments were carried out to accurately determine the porosity and the pore size distribution in the beads.

It was seen that in the volumetric apparatus, the single component CO_2 adsorption in CPO-27–Ni was governed by diffusion through the macropores with contributions from Knudsen and viscous diffusion mechanisms. The binary experiments with the different carrier gases on the ZLC apparatus clearly showed the presence of a macropore diffusion-controlled mechanism and detailed description of these experiments are provided in the subsequent sections of this manuscript.

2 Materials

CPO-27–Ni MOF beads were synthesized by SINTEF by alginate methods and the procedure for synthesis is described in an earlier publication (Spjelkavik et al. 2014). The beads used had a diameter of 3.2 mm. Pure CO_2 (99.8%), He (99.9995%) and N_2 (99.998%) were obtained from BOC Gases, UK.

3 Volumetric method

The adsorption isotherms on the powders and beads were measured on the volumetric system Autosorb iQ from Quantachrome shown in Fig. 1. A known mass of the sample was inserted into a 9 mm measuring cell with a bulb. First, the empty weight of the cell covered with a plug of a known weight was recorded. Then the sample was inserted into the measuring cell and then the total weight of the cell along with the plug was noted. The difference in the two weights provided the mass of the sample. The sample was then regenerated in situ for 14 h under vacuum at 403 K. After regeneration, the sample cell was mounted on to the sample station and the experiments were started in the standard mode, where the gas was dosed several times to achieve the specified equilibrium pressure. Each experiment comprises of measuring the adsorption isotherm up to 100 kPa and desorption back to 0.5 kPa. The whole set up was controlled by the software ASiQwin. The sample was maintained at the experimental temperature by a water bath, which was connected to a Julabo F-25 circulator. The experiments were carried out for three different temperatures viz. 283 K, 308 K and 323 K respectively. In our study, about 1 g of the beads was used. Prior to the volumetric apparatus, the gases were pre-dried using columns packed with Zeolite 5A and silica gel to remove any traces of moisture present. It is important to note that the experiments were also carried out for 263 K and 273 K to obtain the nitrogen isotherms and the isotherms are reported in Fig. 2.

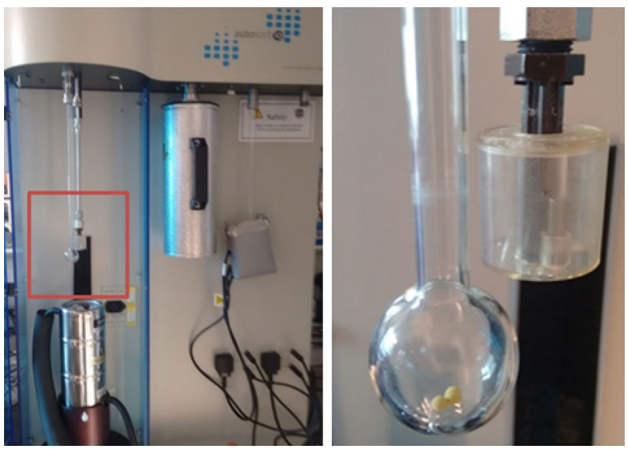

Fig. 1 Autosorb volumetric apparatus (left), two CPO-27–Ni beads used for studying the mass transfer kinetics (right)

Experiments were then carried out at 308 K to study the adsorption kinetics on CPO-27–Ni with two beads as seen from Fig. 1. This was done to minimize heat effects due to adsorption of CO_2 in the sample. In this experiment, a known volume of sorbate (0.5 cm^3) was dosed and the pressure was monitored with time. Once equilibrium was achieved, the next dose was carried out. This mode of operation is called the vector-dose mode, and this is different from the standard mode in the fact that the volume of each dose and the duration of the experiment for each dose were specified. A series of such doses were carried out and, in each case, the transient pressure response in the dosing volume was recorded with time. The transient response was then used to back out the value of the diffusional time constant using a piezometric model and the details are described in subsequent sections.

4 Analysis of the isotherm data

Once the CO_2 and N_2 isotherms shown in Figs. 2 and 3 were obtained, they were then fitted to a dual-site Langmuir isotherm of the form given below by minimizing the residual between the experiment and the model

$$q^* = \frac{q_{s,1} b_{0,1} e^{\frac{-\Delta H_1}{RT}} P}{1 + b_{0,1} e^{\frac{-\Delta H_1}{RT}} P} + \frac{q_{s,2} b_{0,2} e^{\frac{-\Delta H_2}{RT}} P}{1 + b_{0,2} e^{\frac{-\Delta H_2}{RT}} P}, \quad (1)$$

where q_s is the saturation capacity in mmol/g, b_0 is the equilibrium constant in kPa^{-1} and ΔH is the heat of adsorption in J/mol. Subscripts 1 and 2 denote sites 1 and 2 respectively. For the sake of thermodynamic consistency, the saturation capacities of CO_2 and N_2 were kept the same, and the b and the ΔH values were obtained for nitrogen. By looking at

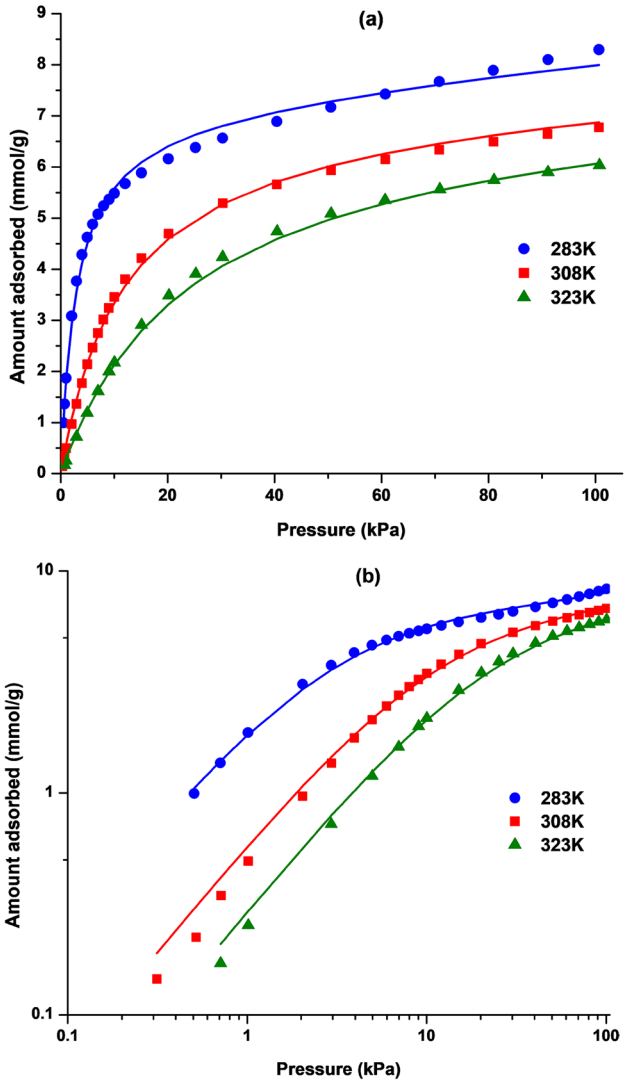

Fig. 2 CO_2 isotherms in **a** linear and **b** log scale in CPO-27–Ni beads. The lines denote dual site Langmuir fits

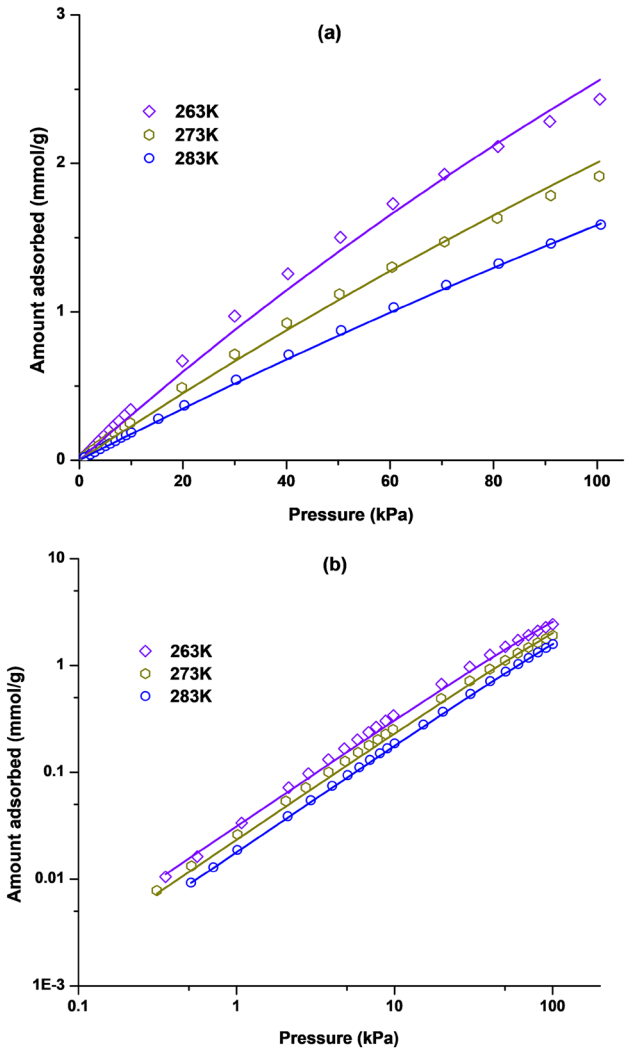

Fig. 3 Nitrogen isotherms in CPO-27–Ni in **a** linear and **b** log scale. The lines denote dual site Langmuir fit

the shape of the nitrogen isotherm in Fig. 3, the isotherm is linear and therefore only one meaningful parameter can be obtained. So, the assumption that the affinities of sites 1 and 2 are equal for nitrogen is made and we only fit two parameters in this case. The adsorption isotherm parameters are shown in Table 1. The sample has a CO_2/N_2 limiting selectivity of 73. This is considerably less than that of Zeolite 13X, which is known to have a CO_2/N_2 selectivity of 1000 (Gibson et al. 2016). From the isotherm parameters, the heat of adsorption of CO_2 and N_2 are found to be − 39.7 and − 17.3 kJ/mol respectively which are consistent with values reported in literature (Chavan et al. 2009; Dietzel et al. 2009; Queen et al. 2014).

5 Volumetric/piezometric method

In this model, the set-up comprises of a dosing cell at a known pressure and an uptake cell, which contains the sample, and a valve connects the two cells. Adsorption takes place when the sorbate is introduced to the uptake cell by opening the valve. Brandani (1998) had developed an analytical solution for the piezometric model considering an isothermal approximation and an ideal valve with zero opening time. The present study adopts this approach to study the mass transfer of CO_2 in CPO-27–Ni.

As mentioned earlier, the uptake measurements were carried out with two beads in the measuring cell with each of the beads being 3.2 mm in diameter. A series of doses of known volume were carried out and the pressure was monitored with time. Once the raw signal was obtained, it was the normalised in the following manner (Brandani et al. 2019).

$$\overline{P} = \frac{P_d(t) - P_{\text{inf}}}{P_{d0} - P_{\text{inf}}}. \tag{2}$$

In this equation, P_d represents the dosing side pressure. Subscripts 0 and inf correspond to the initial and final pressures respectively. The normalised pressure was then compared with the predictions of the model described below. The model accounts for the mass balance in both the dosing and the uptake volume and the flow through the valve with a small pressure steps. The model also assumes that equilibrium exists at the surface between the gas and the solid phases and a linear relationship to describe the adsorption equilibrium. The analytical solution shown in Eqs. 7 and 8 were obtained for spherical particles by introducing the following dimensionless groups.

$$\begin{aligned} &\tau = \frac{tD}{R^2} \quad Q = \frac{q(t) - q_0}{q_\infty - q_0} \quad C = \frac{C(t) - C_0}{C_\infty - C_0} \\ &\rho_D = \frac{P_d(t) - P_U^0}{P_\infty - P_U^0} \quad \rho_U = \frac{P_U(t) - P_U^0}{P_\infty - P_U^0}, \end{aligned} \tag{3}$$

$$\gamma = \frac{1}{3\Delta n_a}\left(\frac{P_{\text{inf}} - P_{u0}}{R_g}\right)\left(\frac{V_{uH}}{T_0} + \frac{V_{uC}}{T_u}\right), \tag{4}$$

$$\delta = \frac{V_d}{3\Delta n_a}\left(\frac{P_{\text{inf}} - P_{u0}}{R_g T_0}\right), \tag{5}$$

$$\omega = \frac{R_g T_d}{V_d}\bar{\chi}\frac{R^2}{D}, \tag{6}$$

$$\frac{\rho_d}{\rho_d^0} = \frac{3\delta}{1 + 3\delta + 3\gamma} + \sum_{i=1}^{\infty} a_i e^{-\beta_i^2 \tau}, \tag{7}$$

$$\frac{\rho_u}{\rho_d^0} = \frac{3\delta}{1 + 3\delta + 3\gamma} + \sum_{i=1}^{\infty} a_i \left(1 - \frac{\beta_i^2}{\omega}\right) e^{-\beta_i^2 \tau}. \tag{8}$$

Here a_i and β_i are given by the equations

$$a_i = \frac{2\omega\delta\beta_i^2}{2\omega\delta\beta_i^2 + (\omega - \beta_i^2)^2 + (\beta_i^2 + z_i^2 - z_i + 2\gamma\beta_i^2)}, \tag{9}$$

$$z_i = 1 + \gamma\beta_i^2 + \frac{\omega\delta\beta_i^2}{\omega - \beta_i^2}. \tag{10}$$

β_i are the positive non-zero roots of

$$\beta_i \cot \beta_i - z_i = 0. \tag{11}$$

Here γ and δ are the ratios of accumulation in the uptake cell and the solid and the dosing cell, the solid respectively, and these are calculated. The instrument measures the hot and cold volume zones of the uptake cell (V_u) i.e., the volume of the cell immersed in the water bath at a constant temperature and the volume of the cell exposed

Table 1 CO_2 and N_2 isotherm parameters for CPO-27–Ni beads

Parameter	CO_2	N_2
$q_{s,1}$ (mol/kg)	7.02	7.02
$b_{0,1}$ (kPa^{-1})	1.5×10^{-8}	8.3×10^{-7}
ΔH_1 (kJ/mol)	− 39.9	− 17.3
$q_{s,2}$ (mol/kg)	6.95	6.95
$b_{0,2}$ (kPa^{-1})	9×10^{-8}	8.3×10^{-7}
ΔH_2 (kJ/mol)	− 23.6	− 17.3
Henry's constant (303 K) (mol/kg/bar)	80.5	1.1
Residual of fitting	0.0042	1.3×10^{-4}

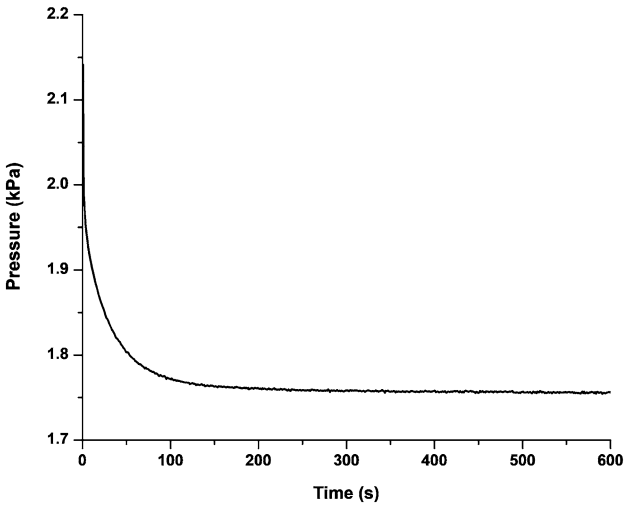

Fig. 4 Transient pressure response in the dosing volume corresponding to an equilibrium pressure of 1.76 kPa

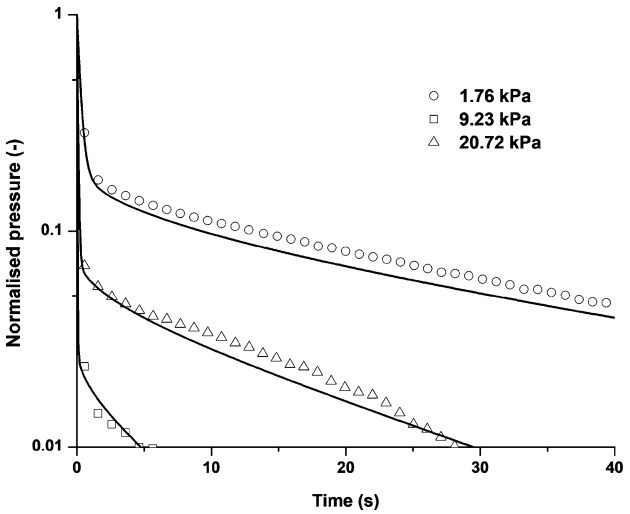

Fig. 5 Normalised pressure curves for three different equilibrium pressure values. The lines denote the analytical solution of the diffusion model

to ambient conditions and the volume of the dosing cell (V_d) and the temperature of the manifold (T_u). Δn_a is the change in the number of moles during the adsorption and therefore this enables us to calculate the value of γ and δ. ω is the valve constant which increases with the pressure.

In the first step, the pressure response shown in Fig. 4 was normalised according to Eq. 2 and the normalised pressure with time is plotted in Fig. 5 for different pressures. By plotting the pressure in this manner, it is possible to distinguish between mass transfer and heat transfer limited mechanisms. As seen from the figure, the uptake profile is a simple exponential suggesting that there is only one time constant. The normalized pressure was then compared to the model solution to obtain the diffusional time constant (R^2/D).

Table 2 Porosimetry values of CPO-27–Ni

Parameter	Value
Porosity	0.383
Mean pore diameter (μm)	0.016

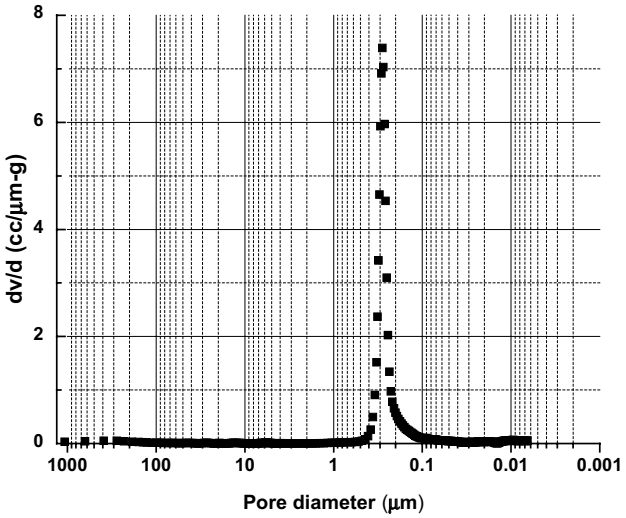

Fig. 6 Pore size distribution in CPO-27–Ni

The kinetic measurements were coupled with independent mercury intrusion experiments to estimate the pore size and the porosity of the CPO-27–Ni beads. The values of the porosity and the pore size are summarized in Table 2 and the pore size distribution is shown in Fig. 6.

6 Analysis of the uptake curves

Figure 5 shows the comparison of the pressure profiles of the experiment and the piezometric model for three different equilibrium pressure points namely 1.76 kPa, 9.23 kPa and 20.72 kPa. The parameters, γ, δ, ω and K along with the initial and final pressures in the dosing and uptake cells are given in Table 3. At the lower pressure, the slope of the isotherm is higher and therefore the values of δ and γ are lower. With an increase in pressure, the slope of the isotherm decreases and therefore the values of δ and γ increase. It can also be seen that the valve constant increases with increase in pressure.

From Fig. 5, the normalised pressure curve is a simple exponential and the slope is the measure of the diffusional time constant. There is a good agreement between the model and the experimental data in the fact that the slopes of the

Table 3 Piezometric model parameters for the transient responses in Fig. 4

P_{inf} (kPa)	P_{d0} (kPa)	Pu_0 (kPa)	K	γ	δ	ω	D/R^2 (s^{-1})
1.76	3.1	1.17	698.3	0.41	0.32	1200	0.0018
9.22	10.41	8.45	270.2	1.6	1.25	1800	0.0048
20.72	21.77	19.92	112.5	4.83	3.8	2500	0.012

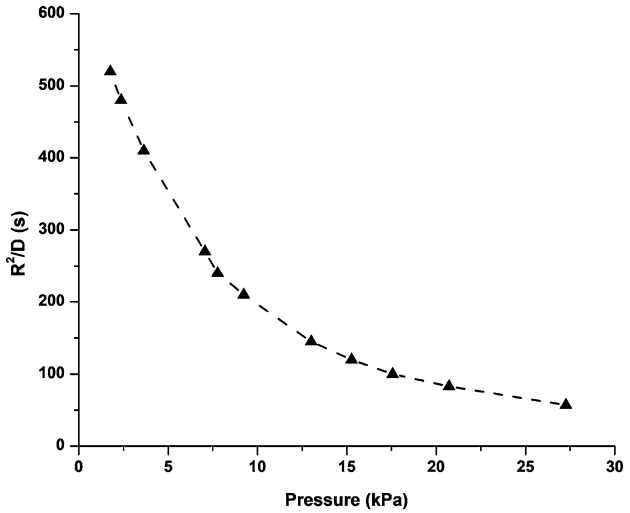

Fig. 7 Diffusional time constants for various pressure steps for CO_2 adsorption in CPO-27–Ni at 308 K. The line is just for guidance only

two curves are identical. Further, the slope of the exponential region increases with increase in pressure, suggesting that the mass transfer is faster at higher pressures.

Figure 7 shows the trend in the diffusional time constant with pressure. The value of diffusivity increases by an order of magnitude from 1.76 kPa, the lowest pressure point to the highest pressure at 27.3 kPa, suggesting that the mass transfer becomes faster with increase in pressure. As the experiments correspond to pure components, the transport mechanism can be due to viscous and Knudsen flow across the macropores and diffusion along the micropores. Given that the micropores of CPO-27–Ni are more than double the kinetic diameter of CO_2, micropore diffusion will be fast and the system will be macropore diffusion controlled. In case of a macropore controlled diffusion process, the uptake curves show an increase in slope with increase in the pressure. This is because the slope of the isotherm decreases with pressure thereby resulting in an increase in the effective macropore diffusivity. At very low pressures, the Knudsen diffusion is dominant, while the viscous contribution becoming significant at high pressures. As these two diffusion regimes occur in parallel, the resultant diffusion coefficient is a sum of the Knudsen and viscous contributions, which are expressed as

$$D_V = \frac{\mathrm{Pr}_{pore}^2}{8\mu}, \tag{12}$$

$$D_{Knudsen} = 9700 r_{pore}\sqrt{\frac{T}{M}}, \tag{13}$$

$$D_K = \frac{9}{13} D_{Knudsen}, \tag{14}$$

$$D_{macro} = D_V + D_K. \tag{15}$$

It should be noted that the Knudsen diffusivity was corrected with the Derjaguin's (Derjaguin 1994; Levitz 1993) expression as seen from Eq. 14.

The effective diffusivity is defined by the equation

$$D_P^e = \frac{\varepsilon_p \frac{D_{macro}}{\tau}}{\varepsilon_p + (1-\varepsilon_p)K}. \tag{16}$$

The tortuosity was obtained by rearranging Eq. 16 in which the effective diffusivity was obtained from the slope of the uptake curves, the macropore diffusivity was obtained from the correlations defined by Eqs. 12 to 15. The value of particle porosity was given by the mercury intrusion experiments and K was obtained from the slope of the isotherm between the start and the end of the dosing. The tortuosity values were obtained for different pressures and are shown in Fig. 8 and summarized in Table 4 for three pressure steps. The average value of tortuosity was found to be 2.7. Using the average tortuosity, the measured and the predicted diffusivity values were compared in Fig. 9 and there seems to be good agreement suggesting that the system is governed by the diffusion through macropores.

From Fig. 7, it can be seen that the time constant for CO_2 adsorption at 10 kPa is approximately of the order of 200 s. For commercial beads of Zeolite 13X, at 10 kPa and at 283 K a value of approximately 48 s was reported (Hu et al. 2014) and at a similar temperature of 308 K, the time constant will be even lower.

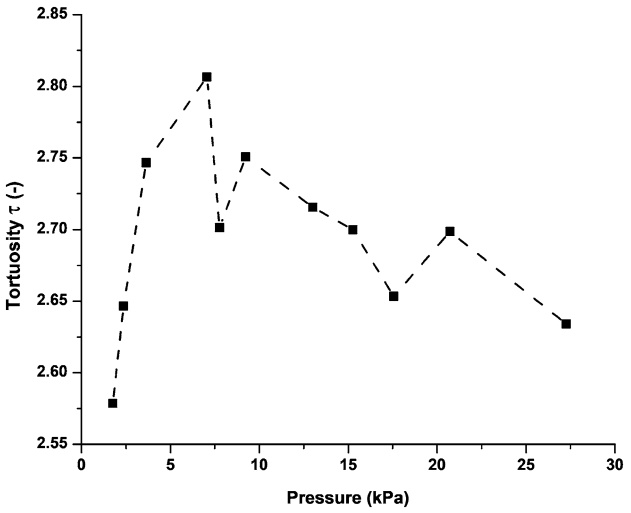

Fig. 8 Estimated tortuosity for different pressure steps. The line is for visualisation only

Table 4 Summary of the volumetric experiments on CPO-27–Ni at 308 K

Pressure (Torr)	D_K (cm^2/s)	D_V (cm^2/s)	$D_V + D_K$ (cm^2/s)	τ
1.76	0.142	0.0008	0.143	2.57
9.22	0.142	0.042	0.146	2.75
20.72	0.142	0.01	0.151	2.7

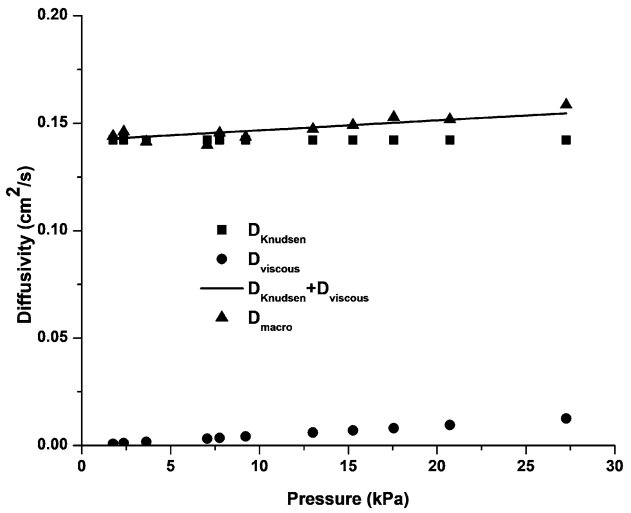

Fig. 9 Comparison of the Knudsen, viscous and macropore diffusivity values. The macropore diffusivity was obtained with a tortuosity value of 2.7

7 Zero length column (ZLC) apparatus

The ZLC adsorption apparatus is an established experimental technique that has been used for nearly 30 years to obtain adsorption equilibrium and kinetics (Brandani et al. 2003; Eic and Ruthven 1988; Hu et al. 2014). In this experiment, a small amount of sample, typically less than 15 mg is first saturated with a gas mixture of a specific composition and then, desorption is carried out with an inert purge gas. By studying the desorption response at different flow rates, it is possible to obtain the information on the mass transfer kinetics. The main advantage of this technique is that due to the small amount of sample used, external mass transfer resistances and heat effects can be eliminated. The column length is shorter, the axial dispersion is therefore large, and the system is analogous to a well-mixed stirred tank reactor. Further, this technique also enables rapid characterization of samples because the experiments can be carried out at different flow rates, using different carrier gases and at different temperatures.

Brandani and Ruthven (1995) had developed the following analytical solution for the ZLC assuming Fickian diffusion in spherical particles

$$\frac{C}{C_0} = 2L \sum_{n=1}^{\infty} \frac{\exp\left(-\beta_n^2 \frac{D}{R^2} t\right)}{\beta_n^2 + (L - 1 - \gamma_Z \beta_n^2)^2 + L - 1 + \gamma_Z \beta_n^2}. \quad (17)$$

Here β_n are the roots of the equation

$$\beta_n \cot \beta_n + L - 1 - \gamma_Z \beta_n^2 = 0. \quad (18)$$

L is the ratio of the diffusional time constant and the convective desorption time constant and γ_Z is the ratio of the hold up in the fluid phase to the accumulation in the solid phase. When $L < 1$, the system is under equilibrium controlled and kinetically controlled when L is far greater than 1 (Friedrich et al. 2015). The linear model can be used to obtain initial estimates of the diffusivity that can be used for the more refined analysis described in the section that follows.

The ZLC apparatus used in this study is shown in Fig. 10 and has been described in detail in an earlier publication (Hu et al. 2015a). It consists of a SANYO 212 oven where the mixture of a certain composition is prepared, the ZLC oven (Carbolite) which contains the column and an AMETEK benchtop quadrupole mass spectrometer. The ZLC is a Swagelok 1/4″ to 1/8″ reducing union shown in Fig. 10 and was packed with a single 3.2 mm bead weighing 8 mg.

Prior to the experiment, the sample was regenerated in a helium purge of 10 cm^3/min overnight. Experiments were then carried out at 35 °C by saturating the sample with a 10% CO_2–helium mixture for followed by desorption with a pure helium purge. This was carried out at different flow rates to identify whether the system was equilibrium controlled or limited by the mass transfer kinetics and initial

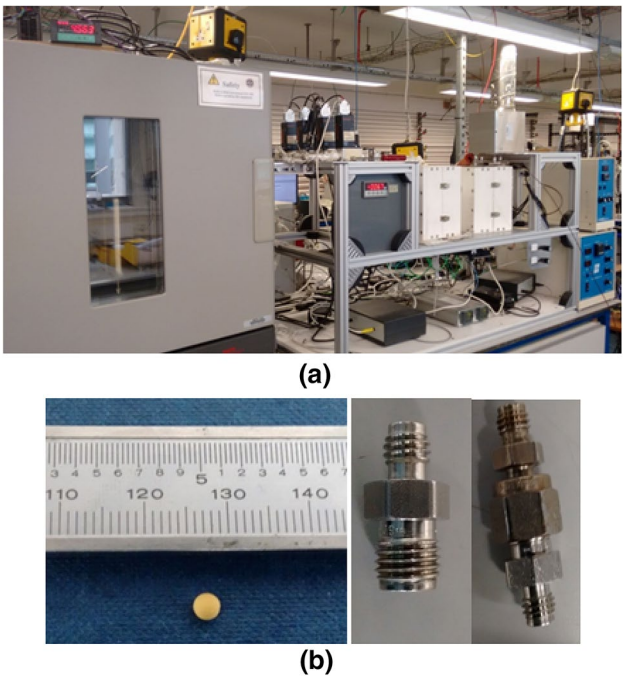

Fig. 10 **a** Semi-automated zero length column (ZLC) apparatus used in this study and **b** 3.2 mm bead used for the ZLC experiments (left) and zero length column (right)

estimates of the values of the diffusivities were obtained from the slope of the long-time asymptote.

To identify the transport mechanism, experiments were then conducted with nitrogen as a carrier gas. If the system was under macropore diffusion-controlled regime, then the slope of the long-time region would depend on the carrier gas, due to the difference in molecular diffusivities. The experimental curves with different carrier gases would be identical if the diffusion through the micropores was the dominant transport mechanism.

8 Analysis of the ZLC curves

The ZLC experiments were carried out with a 10% CO_2–He mixture for different flow rates. Experiments were first carried out at low flow rates and the isotherm up to 10 kPa was obtained by performing a mass balance on the desorption curves and subtracting the blank responses. The adsorption isotherm thus obtained is about 8% lower than the isotherm obtained from the volumetric experiment. The difference between the isotherms obtained from the volumetric apparatus and the ZLC, can be attributed to the fact that a single bead was used in the ZLC experiment, which can be different from the beads used in the other experiment.

In the next step, experiments were carried out at higher flow rates namely 20 cm^3 and 30 cm^3 respectively. To

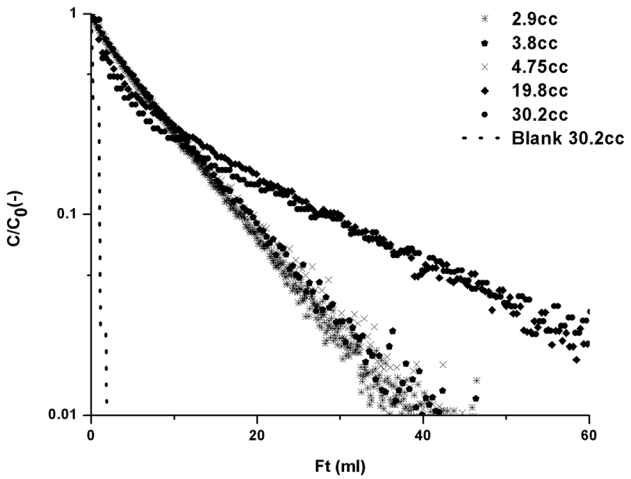

Fig. 11 Ft (Flow rate × time) plot at different flow rates for a 10% CO_2–helium mixture

establish whether the system was in equilibrium or kinetically controlled regime, a plot of the flowrate times time vs the normalised concentration was obtained and are shown in Fig. 11. As seen from the figure, the curves corresponding to flow rates up to 20 cm^3/min overlap in the entire range suggesting that the system is equilibrium controlled. The curves corresponding to 20 cm^3/min and 30 cm^3/min cross the low flow rate curves and diverge. This is an indication that the system is kinetically controlled, and the values of the diffusivities can be extracted from the slope of the long-time asymptote.

If the mass transfer is governed by the diffusion through macropores, then the slope of the long-time asymptote changes with carrier gas. Therefore, experiments were then

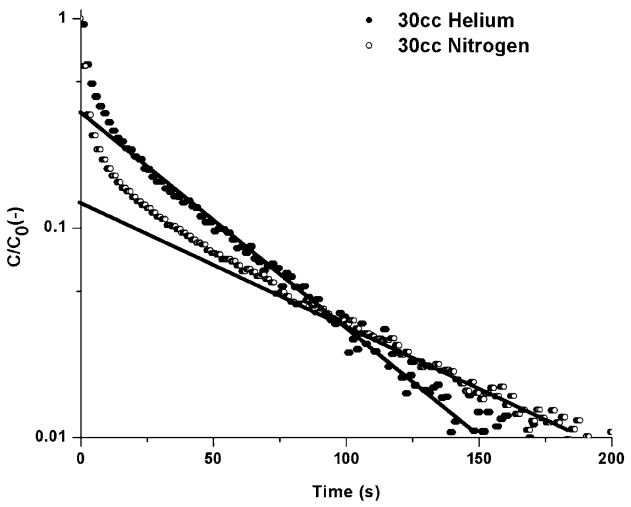

Fig. 12 Comparison of 10% CO_2–He and 10% CO_2–N_2 experiment at 30 cm^3/min. The solid lines are for visualizing the change in the slope of the long-time asymptote with the carrier gas

carried out with a 10% CO_2 in N_2 mixture. As seen from the slopes in Fig. 12, the slope of the long-time asymptote in case of the helium experiment is higher than that of the nitrogen experiment, suggesting that the system in macropore diffusion controlled. This agrees with previous work that have characterized this material for CO_2 adsorption kinetics (Hu et al. 2015a; Liu et al. 2010).

The diffusivity values were then extracted by simultaneously fitting the 20 cm^3 and 30 cm^3 experiments using an automated ZLC fitting tool (Friedrich et al. 2015). The automated ZLC fitting tool is a Python script which used genetic algorithm to minimize the residual between the experiment and the model. The ZLC experiment is simulated using CySim, an adsorption cycle simulator developed at the University of Edinburgh (Friedrich et al. 2013). The CySim code is written in a modular form and accounts for the valves, adsorption columns, splitters, etc. The system of differential algebraic equations is solved in SUNDIALS. For simulating the ZLC, the component mass balance, macropore diffusion and micropore LDF models are considered and the detector is treated as a CSTR. The column is under isothermal conditions and there is no pressure drop across the column.

In the first step, blank and the packed experimental data corresponding to the low flowrate experiments were fitted to obtain the CO_2 isotherm. In the next step, the high flowrate experiments were then simulated using the isotherm obtained in the previous step and the effective diffusivity calculated from the particle porosity obtained from the mercury intrusion experiments and the tortuosity obtained from the volumetric experiments. As mentioned before, the CO_2 isotherm obtained from the ZLC experiment was 8% lower than the isotherm obtained from volumetry. The same scaling factor was obtained for the nitrogen isotherm and the isotherm was then used in the ZLC fitting tool to fit the CO_2–N_2 experiments.

In case of a ZLC experiment, the macropore diffusion is a combination of Knudsen and molecular diffusivities. Since the total pressure of the system is constant, the contribution from the viscous diffusion can be neglected. The combined macropore diffusivity in this case is given by

$$\frac{1}{D_{macro}} = \frac{1}{D_M} + \frac{1}{D_K}. \tag{19}$$

The molecular diffusivity can be obtained from the Chapman–Enskog (Bird et al. 2002) correlation as shown in equation

$$D_M = \frac{0.001858T^{3/2}}{P\sigma_{1,2}^2\Omega}\left(\sqrt{\frac{1}{M_1}+\frac{1}{M_2}}\right). \tag{20}$$

The comparison between the experiment and the simulated ZLC curves are shown in Figs. 13 and 14 with good agreement between the experiment and simulation. The results are summarized in Table 5. The tortuosity value agrees well with the average value obtained from the volumetric experiment.

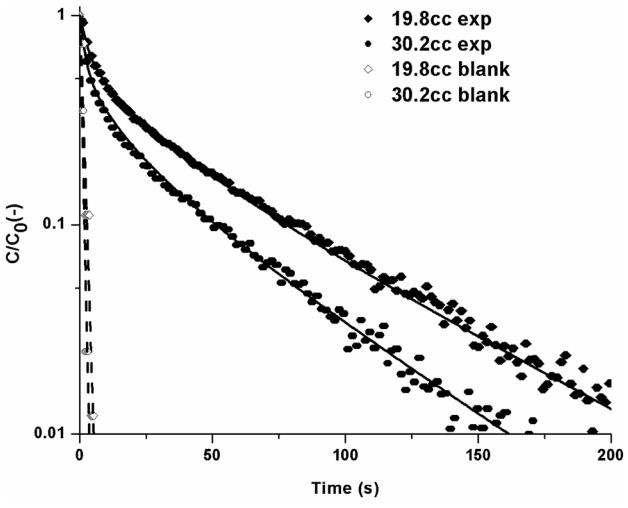

Fig. 13 Experiment (symbols) and simulated (lines) ZLC curves at 20 and 30 cm^3/min for a 10% CO_2–He mixture

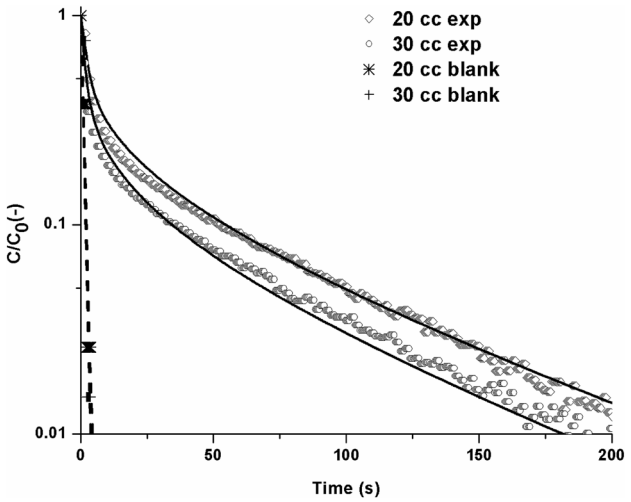

Fig. 14 Experiment (symbols) and simulated (lines) ZLC curves at 20 and 30 cm^3/min for a 10% CO_2–N_2 mixture

Table 5 Summary of the ZLC experiments on CPO-27–Ni at 308 K

Carrier gas	$\varepsilon_P D_{macro}/\tau$ (cm^2/s)	D_M (cm^2/s)	D_K (cm^2/s)	D_{macro} (cm^2/s)	τ
Helium	0.017	0.651	0.142	0.116	2.67
Nitrogen	0.011	0.165	0.142	0.077	2.74

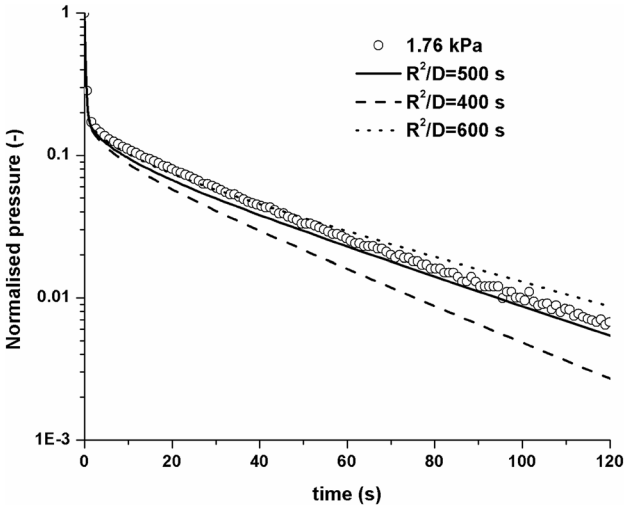

Fig. 15 Volumetric curve at 1.76 kPa with the calculated curves including ± 20% in the diffusion time constant

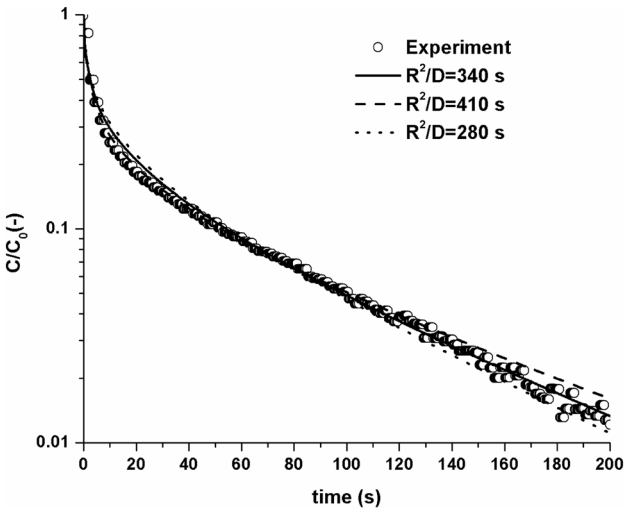

Fig. 16 ZLC curve at 20 cm^3/min for a 10% CO_2–N_2 mixture with the calculated curves including ± 20% in the diffusion time constant

9 Uncertainty in the measured diffusional time constants

The diffusion time constants are estimated matching the theoretical models to the experimental data. In both the ZLC and the volumetric systems a typical uncertainty is ± 10%. This is reflected in the variance of the calculated tortuosity reported in Fig. 8. Additionally, Figs. 15 and 16 show an example of a volumetric and a ZLC curve respectively with the fitted diffusion time constants and the corresponding model predictions with an uncertainty of ± 20% in the diffusivity. The data are well within this range and given that the slope of the long-time asymptotes is directly proportional to the diffusivity the actual uncertainty is clearly less than 20% and close to ± 10%.

10 Conclusions

Adsorption isotherms of CO_2 and N_2 were measured in the CPO-27–Ni sample. It was seen that the adsorption capacity of CO_2 was significantly higher than that of nitrogen. The isotherms were then fitted to a dual-site Langmuir model. In the next step, uptake measurements were carried out to obtain the time constants for CO_2 adsorption in the beaded sample. The pressure versus time curve was obtained from the uptake measurements were first normalised and a piezometric model was then used to back out the diffusional time constants for a series of curves corresponding to the partial pressure of CO_2 in a vacuum swing adsorption process. From this methodology, the macropore diffusion described by Knudsen and viscous flow is the dominant mechanism in CPO-27–Ni and the tortuosity was found to be 2.7. Binary experiments carried out with 10% CO_2–He and 10% CO_2–N_2 mixtures showed that the long-time asymptote at higher flow rates was a function of the carrier gas indicating that the system was macropore diffusion controlled.

Acknowledgements The authors would like to acknowledge funding from the Engineering and Physical Sciences Research Council, Grant EP/L021064/1: Post-Combustion Carbon Capture Using MOFs: Materials and Process Development. SINTEF would like to acknowledge Internal Project 102005015-49 for the preparation of the manuscript.

References

Al Haydar, M., Abid, H.R., Sunderland, B., Wang, S.: Metal organic frameworks as a drug delivery system for flurbiprofen. Drug Des. Dev. Ther. **11**, 2685–2695 (2017)

Bird, B.R., Stewart, W.E., Lightfoot, E.N.: Transport Phenomena. Wiley, New York (2002)

Brandani, F., Ruthven, D., Coe, C.G.: Measurement of adsorption equilibrium by the zero length column (ZLC) technique Part 1: single-component systems. Ind. Eng. Chem. Res. **42**, 1451–1461 (2003)

Brandani, S.: Analysis of the piezometric method for the study of diffusion in microporous solids: isothermal case. Adsorption **4**, 17–24 (1998)

Brandani, S., Brandani, F., Mangano, E., Pullumbi, P.: Using a volumetric apparatus to identify and measure the mass transfer

resistance in commercial adsorbents. Microporous Mesoporous Mater. (2019). https://doi.org/10.1016/j.micromeso.2019.01.015
Brandani, S., Ruthven, D.M.: Analysis of ZLC desorption curves for liquid systems. Chem. Eng. Sci. **50**, 2055–2059 (1995)
Chavan, S., Bonino, F., Vitillo, J.G., Groppo, E., Lamberti, C., Dietzel, P.D.C., Zecchina, A., Bordiga, S.: Response of CPO-27–Ni towards CO, N_2 and C_2H_4. Phys. Chem. Chem. Phys. **11**, 9811–9822 (2009)
Derjaguin, B.: Measurement of the specific surface of porous and disperse bodies by their resistance to the flow of rarafied gases. Prog. Surf. Sci. **45**, 337–340 (1994)
Dietzel, P.D.C., Besikiotis, V., Blom, R.: Application of metal-organic frameworks with coordinatively unsaturated metal sites in storage and separation of methane and carbon dioxide. J. Mater. Chem. **19**, 7362–7370 (2009)
Dietzel, P.D.C., Georgiev, P.A., Eckert, J., Blom, R., Strassle, T., Unruh, T.: Interaction of hydrogen with accessible metal sites in the metal-organic frameworks M_2(dhtp) (CPO-27–M; M = Ni, Co, Mg). Chem. Commun. **46**, 4962–4964 (2010)
Eic, M., Ruthven, D.M.: A new experimental technique for measurement of intracrystalline diffusivity. Zeolites **8**, 40–45 (1988)
Friedrich, D., Ferrari, M.-C., Brandani, S.: Efficient simulation and acceleration of convergence for a dual piston pressure swing adsorption system. Ind. Eng. Chem. Res. **52**, 8897–8905 (2013)
Friedrich, D., Mangano, E., Brandani, S.: Automatic estimation of kinetic and isotherm parameters from ZLC experiments. Chem. Eng. Sci. **126**, 616–624 (2015)
Furukawa, H., Cordova, K.E., O'Keeffe, M., Yaghi, O.M.: The chemistry and applications of metal-organic frameworks. Science (2013). https://doi.org/10.1126/science.1230444
Gibson, J.A.A., Mangano, E., Shiko, E., Greenaway, A.G., Gromov, A.V., Lozinska, M.M., Friedrich, D., Campbell, E.E.B., Wright, P.A., Brandani, S.: Adsorption materials and processes for carbon capture from gas-fired power plants: AMPGas. Ind. Eng. Chem. Res. **55**, 3840–3851 (2016)
Gygi, D., Bloch, E.D., Mason, J.A., Hudson, M.R., Gonzalez, M.I., Siegelman, R.L., Darwish, T.A., Queen, W.L., Brown, C.M., Long, J.R.: Hydrogen storage in the expanded pore metal-organic frameworks M_2(dobpdc) (M = Mg, Mn, Fe, Co, Ni, Zn). Chem. Mater. **28**, 1128–1138 (2016)
Hindocha, S., Poulston, S.: Study of the scale-up, formulation, ageing and ammonia adsorption capacity of MIL-100(Fe), Cu-BTC and CPO-27(Ni) for use in respiratory protection filters. Faraday Discuss. **201**, 113–125 (2017)
Hu, X., Brandani, S., Benin, A.I., Willis, R.R.: Development of a semiautomated zero length column technique for carbon capture applications: rapid capacity ranking of novel adsorbents. Ind. Eng. Chem. Res. **54**, 6772–6780 (2015a)
Hu, X., Brandani, S., Benin, A.I., Willis, R.R.: Development of a semiautomated zero length column technique for carbon capture applications: study of diffusion behavior of CO_2 in MOFs. Ind. Eng. Chem. Res. **54**, 5777–5783 (2015b)
Hu, X., Brandani, S., Benin, A.I., Willis, R.R.: Testing the stability of novel adsorbents for carbon capture applications using the zero length column technique. Chem. Eng. Res. Des. **131**, 406–413 (2018)
Hu, X., Mangano, E., Friedrich, D., Ahn, H., Brandani, S.: Diffusion mechanism of CO_2 in 13X zeolite beads. Adsorption **20**, 121–135 (2014)
Khurana, M., Farooq, S.: Simulation and optimization of a 6-step dual-reflux VSA cycle for post-combustion CO_2 capture. Chem. Eng. Sci. **152**, 507–515 (2016)
Kizzie, A.C., Wong-Foy, A.G., Matzger, A.J.: Effect of humidity on the performance of microporous coordination polymers as adsorbents for CO_2 capture. Langmuir **27**, 6368–6373 (2011)
Krishnamurthy, S., Haghpanah, R., Rajendran, A., Farooq, S.: Simulation and optimization of a dual-adsorbent, two-bed vacuum swing adsorption process for CO_2 capture from wet flue gas. Ind. Eng. Chem. Res. **53**, 14462–14473 (2014a)
Krishnamurthy, S., Rao, V.R., Guntuka, S., Sharratt, P., Haghpanah, R., Rajendran, A., Amanullah, M., Karimi, I.A., Farooq, S.: CO_2 capture from dry flue gas by vacuum swing adsorption: a pilot plant study. AIChE J. **60**, 1830–1842 (2014b)
Levitz, P.: Knudsen diffusion and excitation transfer in random porous media. J. Phys. Chem. **97**, 3813–3818 (1993)
Li, G., Xiao, P., Webley, P., Zhang, J., Singh, R., Marshall, M.: Capture of CO_2 from high humidity flue gas by vacuum swing adsorption with zeolite 13X. Adsorption **14**, 415–422 (2008)
Liu, J., Benin, A.I., Furtado, A.M.B., Jakubczak, P., Willis, R.R., LeVan, M.D.: Stability effects on CO_2 adsorption for the DOBDC series of metal-organic frameworks. Langmuir **27**, 11451–11456 (2011)
Liu, J., Wang, Y., Benin, A.I., Jakubczak, P., Willis, R.R., LeVan, M.D.: CO_2/H_2O adsorption equilibrium and rates on metal-organic frameworks: HKUST-1 and Ni/DOBDC. Langmuir **26**, 14301–14307 (2010)
Lustig, W.P., Mukherjee, S., Rudd, N.D., Desai, A.V., Li, J., Ghosh, S.K.: Metal-organic frameworks: functional luminescent and photonic materials for sensing applications. Chem. Soc. Rev. **46**, 3242–3285 (2017)
Mangano, E., Kahr, J., Wright, P.A., Brandani, S.: Accelerated degradation of MOFs under flue gas conditions. Faraday Discuss. **192**, 181–195 (2016)
Mason, J.A., Veenstra, M., Long, J.R.: Evaluating metal-organic frameworks for natural gas storage. Chem. Sci. **5**, 32–51 (2014)
Pato-Doldán, B., Rosnes, M.H., Dietzel, P.D.C.: An in-depth structural study of the carbon dioxide adsorption process in the porous metal-organic frameworks CPO-27–M. ChemSusChem **10**, 1710–1719 (2017)
Pettinari, C., Marchetti, F., Mosca, N., Tosi, G., Drozdov, A.: Application of metal–organic frameworks. Polym. Int. **66**, 731–744 (2017)
Queen, W.L., Hudson, M.R., Bloch, E.D., Mason, J.A., Gonzalez, M.I., Lee, J.S., Gygi, D., Howe, J.D., Lee, K., Darwish, T.A., James, M., Peterson, V.K., Teat, S.J., Smit, B., Neaton, J.B., Long, J.R., Brown, C.M.: Comprehensive study of carbon dioxide adsorption in the metal–organic frameworks M_2(dobdc) (M = Mg, Mn, Fe, Co, Ni, Cu, Zn). Chem. Sci. **5**, 4569–4581 (2014)
Rajagopalan, A.K., Avila, A.M., Rajendran, A.: Do adsorbent screening metrics predict process performance? A process optimisation based study for post-combustion capture of CO_2. Int. J. Greenh. Gas Control **46**, 76–85 (2016)
Ranocchiari, M., van Bokhoven, J.A.: Catalysis by metal-organic frameworks: fundamentals and opportunities. Phys. Chem. Chem. Phys. **13**, 6388–6396 (2011)
Spjelkavik, A.I., Arya, A., Divekar, S., Didriksen, T., Blom, R.: Forming MOFs into spheres by use of molecular gastronomy methods. Chem. Eur. J. **20**, 8973–8978 (2014)
Tagliabue, M., Rizzo, C., Millini, R., Dietzel, P.D.C., Blom, R., Zanardi, S.: Methane storage on CPO-27–Ni pellets. J. Porous Mater. **18**, 289–296 (2011)
Youssef, P.G., Dakkama, H., Mahmoud, S.M., Al-Dadah, R.K.: Experimental investigation of adsorption water desalination/cooling system using CPO-27Ni MOF. Desalination **404**, 192–199 (2017)
Zhang, Y., Feng, X., Yuan, S., Zhou, J., Wang, B.: Challenges and recent advances in MOF–polymer composite membranes for gas separation. Inorg. Chem. Front. **3**, 896–909 (2016)